Dalton Transactions

PAPER

View Article Online
View Journal | View Issue

Cite this: *Dalton Trans.*, 2014, **43**, 15491

Behavior of anionic molybdenum(IV, VI) and tungsten(IV, VI) complexes containing bulky hydrophobic dithiolate ligands and intramolecular NH···S hydrogen bonds in nonpolar solvents†

Yuki Hasenaka, Taka-aki Okamura,* Miki Tatsumi, Naoya Inazumi and Kiyotaka Onitsuka

Received 4th June 2014,
Accepted 22nd August 2014

DOI: 10.1039/c4dt01646g

www.rsc.org/dalton

Molybdenum(IV, VI) and tungsten(IV, VI) complexes, $(Et_4N)_2[M^{IV}O\{1,2\text{-}S_2\text{-}3,6\text{-}(RCONH)_2C_6H_2\}_2]$ and $(Et_4N)_2[M^{VI}O_2\{1,2\text{-}S_2\text{-}3,6\text{-}(RCONH)_2C_6H_2\}_2]$ (M = Mo, W; R = $(4\text{-}^tBuC_6H_4)_3C$), with bulky hydrophobic dithiolate ligands containing NH···S hydrogen bonds were synthesized. These complexes are soluble in nonpolar solvents like toluene, which allows the detection of unsymmetrical coordination structures and elusive intermolecular interactions in solution. The ^1H NMR spectra of the complexes in toluene-d_8 revealed an unsymmetrical coordination structure, and proximity of the counterions to the anion moiety was suggested at low temperatures. The oxygen-atom-transfer reaction between the molybdenum(IV) complex and Me_3NO in toluene was considerably accelerated in nonpolar solvents, and this increase was attributed to the favorable access of the substrate to the active center in the hydrophobic environment.

Introduction

Molybdo- and tungstoenzymes with unique dithiolene ligands called the molybdopterin cofactor (MGD, Chart 1a) catalyze oxygen-atom-transfer (OAT) reactions *via* M^{IV} and M^{VI} oxidation states (M = Mo, W).[1–8] In the case of dimethyl sulfoxide reductase (DMSOR), a molybdoenzyme with two dithiolene ligands, the molybdenum(IV) center reductively eliminates an oxygen atom from sulfoxides and amine *N*-oxides to form a Mo^{VI}═O bond.[9] The active site is located at the bottom of a large depression and is buried within the protein matrix, and the coordinating ligands are not exposed to the surface. The hydrophobic pocket formed by aromatic residues at the base of the substrate access funnel is conserved in both DMSOR and trimethylamine *N*-oxide reductase, which suggests the importance of hydrophobicity in the enzyme activity.[1]

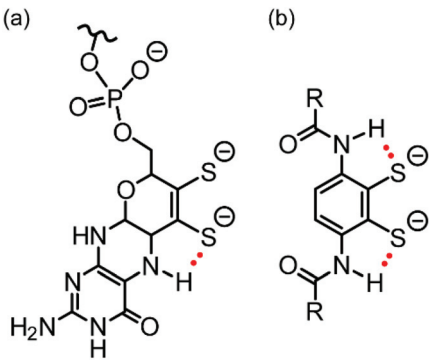

Chart 1 Structures of (a) the molybdopterin cofactor (MGD) and (b) model ligand with intramolecular NH···S hydrogen bonds.

A hydrophobic environment around the active site should support weak interactions such as the binding of substrates and hydrogen bonds, and is probably important for controlling the electrochemical properties. From this point of view, encapsulation using very bulky dendritic molecules has been reported as models of iron–sulfur proteins, heme proteins, and molybdoenzymes.[10–15]

As one of the weak interactions, hydrogen bonds are known to be supported in nonpolar solvents, and the contribution of the NH···S hydrogen bond to the redox potential has been clearly shown, in iron–sulfur peptide model complexes, to be dependent on the polarity of solvents.[16] Our systematic studies

Department of Macromolecular Science, Graduate School of Science, Osaka University, Toyonaka, Osaka 560-0043, Japan.
E-mail: tokamura@chem.sci.osaka-u.ac.jp; Fax: +81 6 6850 5474; Tel: +81 6 6850 5451

† Electronic supplementary information (ESI) available: Synthesis of ligand precursors, structural determination, X-ray crystallographic data, molecular structures of **L1**, **1-Mo**, and **2-W**, the proposed mechanism producing **L1**, IR spectra of **2-W**, resonance Raman spectra of **2-M**, VT NMR spectra of **1-Mo**, and TOCSY and ROESY spectra of **2-W**. CCDC 998963 (**L1**·3.1CH_3OH·H_2O), 998964 (**1-Mo**·8(toluene)), 998965 (**2-Mo**·5CH_3CN), 1006103 (**1-Mo**·toluene·5CH_3CN), 1006104 (**1-W**·4(toluene)·3CH_3CN·H_2O) and 1006105 (**2-W**·5CH_3CN). For ESI and crystallographic data in CIF or other electronic format see DOI: 10.1039/c4dt01646g

using simple model complexes including iron–sulfur proteins,[16–19] cytochrome P450s,[20,21] copper proteins,[22] and molybdo- and tungstoenzymes[23–27] have revealed the positive shift of redox potential by NH···S hydrogen bonds.

A number of complexes have been synthesized to model molybdo- and tungstoenzymes.[28–33] As functional models, monooxomolybdenum(IV) benzene-1,2-dithiolate complexes can eliminate the oxygen atom of trimethylamine *N*-oxide to afford a Mo^{VI}=O bond of dioxomolybdenum(VI) complexes[34,35] although DMSOR uses desoxomolybdenum(IV) and monooxomolybdenum(VI) species. In the research on the NH···S hydrogen bonds of molybdenum benzene-1,2-dithiolate derivatives, we found that the hydrogen bonds accelerate the OAT reaction between Mo^{IV} complexes and Me_3NO and stabilize the resulting Mo^{VI}=O bonds through a *trans* influence.[23,25–27] These suggestive results inspired us to propose the presence of an intra-ligand NH···S hydrogen bond in the pterin cofactor although the NH proton was not observed in crystal structures (Chart 1). As described in detail in our previous papers,[23,27] introduction of four bulky triphenylacetylamino groups into the model complex, *i.e.* $(Et_4N)_2[Mo^{IV}O\{1,2\text{-}S_2\text{-}3,6\text{-}(Ph_3CCONH)_2C_6H_2\}_2]$ (**5-Mo**, Chart 2), resulted in a dramatic acceleration of the OAT reaction *via* the stabilization of a distorted intermediate by the bulky substituents and intramolecular NH···S hydrogen bonds.[23,36] In the proposed mechanism, the substrate approaches the polar molybdenum center from the upper side, *i.e. cis* to the oxo ligand, and spontaneously a Mo=O bond is formed, similarly to the enzyme. If the polar reactive site is covered with hydrophobic media, the vacant site probably simulates the hydrophobic pocket of the active site in molybdoenzymes; however, the low solubility of **5-Mo** in nonpolar solvents prevents us from confirming this hypothesis. Encapsulation of counterions using hydrophobic groups is one solution. In a previous paper, we used the $(4\text{-}^tBuC_6H_4)_3CCONH$ group and found that the two substituents partially masked the ionic molybdenum center and created a hydrophobic environment in $(Et_4N)_2[Mo^{IV}O\{1,2\text{-}S_2\text{-}3\text{-}(4\text{-}^tBuC_6H_4)_3CCONHC_6H_3\}_2]$.[27]

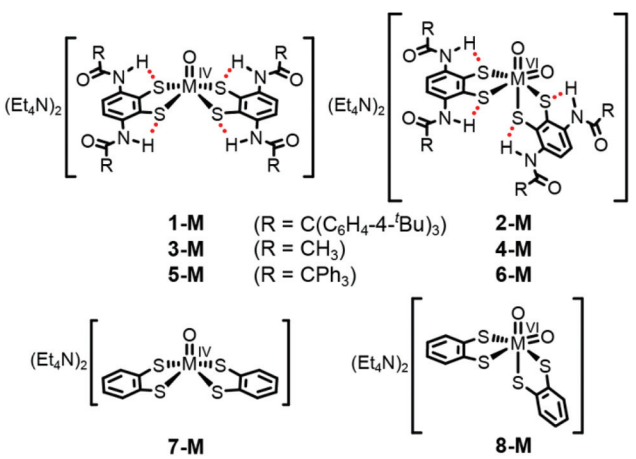

Chart 2 Designation of molybdenum and tungsten complexes (M = Mo, W).

However, the complex was insoluble in nonpolar solvents because of insufficient encapsulation. These results and simulations suggested that introduction of four substituent groups must cover up the ionic parts as shown in this paper. Another approach to understand the effect of a protein matrix at the active site has already been reported by Basu *et al.* using dendritic molecules.[14,15]

Here, molybdenum(IV, VI) and tungsten(IV, VI) complexes (**1-M**, **2-M**; M = Mo, W; Chart 2) containing bulky hydrophobic dithiolate ligands and intramolecular NH···S hydrogen bonds, which make the complexes soluble in nonpolar solvents like toluene, are reported. The OAT reaction of Me_3NO proceeded faster in nonpolar solvents, which demonstrated that the polar substrate had better access to the active center in hydrophobic surroundings. In addition, the solid and solution state structures of the complexes were spectroscopically investigated in detail.

Experimental

All procedures were performed under an argon atmosphere by the Schlenk technique. All solvents were dried and distilled under argon before use. Reagents were obtained commercially and used without further purification. $(4\text{-}^tBuC_6H_4)_3CCOOH$,[27] $3,6\text{-}(NH_2)_2C_6H_2\text{-}1,2\text{-}(SSO_3K)_2$,[37] $(Et_4N)[Mo^VO(SPh)_4]$,[38] and $(Et_4N)[W^VO(SPh)_4]$[39] were prepared by reported methods. The syntheses of $(4\text{-}^tBuC_6H_4)_3CCOCl$, $(4\text{-}^tBuC_6H_4)_3CCONHPh$, $(^nBu_4N)_2[3,6\text{-}(NH_2)_2C_6H_2\text{-}1,2\text{-}(SSO_3)_2]$, and $(^nBu_4N)_2[3,6\text{-}\{(4\text{-}^tBuC_6H_4)_3CCONH\}_2C_6H_2\text{-}1,2\text{-}(SSO_3)_2]$ are shown in ESI.†

$1,2\text{-}S_3\text{-}3,6\text{-}\{(4\text{-}^tBuC_6H_4)_3CCONH\}_2C_6H_2$ (L1)

This compound was synthesized by a modified method reported in the literature.[40] A suspension of $(^nBu_4N)_2[3,6\text{-}\{(4\text{-}^tBuC_6H_4)_3CCONH\}_2C_6H_2\text{-}1,2\text{-}(SSO_3)_2]$ (1.51 g, 889 μmol) and $(NH_2)_2CS$ (129 mg, 1.69 mmol) in AcOH (15 mL) was heated at 100 °C to afford a light yellow solution, and the reaction mixture was stirred for 5 h. The resulting light yellow powder was filtered off, washed with MeOH, and recrystallized from CH_2Cl_2–MeOH to afford yellow blocks. Yield: 539 mg, 56%. Mp: >300 °C. Anal. Calcd for $C_{70}H_{82}N_2O_2S_3$: C, 77.88; H, 7.66; N, 2.59. Found: C, 77.68; H, 7.65; N, 2.87. ^1H NMR ($CDCl_3$): δ 7.62 (s, 2H, NH), 7.42 (s, 2H, 4,5-H), 7.32 (d, J = 8.6 Hz, 12H, Ar), 7.20 (d, J = 8.6 Hz, 12H, Ar), 1.30 (s, 54H, ^{t}Bu). IR (KBr): 3358 (ν_{NH}), 1696 ($\nu_{C=O}$) cm^{-1}.

$(Et_4N)_2[Mo^{IV}O(1,2\text{-}S_2\text{-}3,6\text{-}\{(4\text{-}^tBuC_6H_4)_3CCONH\}_2C_6H_2)_2]$ (1-Mo)

A suspension of **L1** (237 mg, 219 μmol) and Et_4NBH_4 (85 mg, 586 μmol) in a mixture of acetonitrile (5 mL) and water (0.5 mL) was heated at 70 °C for 0.5 h to afford a greenish-yellow solution and a colorless precipitate. After adding acetonitrile (19 mL) to dissolve the precipitate, a solution of $(Et_4N)[Mo^VO(SPh)_4]$ (38.0 mg, 56.0 μmol) in acetonitrile (3 mL) was added dropwise to afford an orange suspension. The reaction mixture was stirred for 72 h at 30 °C to afford a yellow solution and a yellowish-white precipitate. The supernatant was

removed, and the precipitate was washed several times with acetonitrile by centrifugation. The product was extracted with toluene and recrystallized from toluene–acetonitrile to afford yellow blocks. Yield: 66.0 mg, 48%. ^{1}H NMR (toluene-d_8): δ 8.95 (s, 4H, NH), 8.18 (s, 4H, 4,5-H), 7.70 (d, J = 8.4 Hz, 24H, Ar), 7.37 (d, J = 8.4 Hz, 24H, Ar), 1.88 (br, 16H, Et_4N^+), 1.31 (s, 108H, ^{t}Bu), 0.37 (br, 24H, Et_4N^+). ^{1}H NMR (DMF-d_7): δ 9.10 (s, 4H, NH), 8.02 (s, 4H, 4,5-H), 7.43 (d, J = 8.7 Hz, 24H, Ar), 7.38 (d, J = 8.7 Hz, 24H, Ar), 3.21 (q, J = 7.3 Hz, 16H, Et_4N^+), 1.26 (s, 108H, ^{t}Bu), 1.17 (tt, J_{H-H} = 7.3 Hz, J_{H-N} = 1.6 Hz, 24H, Et_4N^+). ESI-MS (CH_3CN) calcd for $[Mo^{IV}O(1,2\text{-}S_2\text{-}3,6\text{-}\{(4\text{-}^tBuC_6H_4)_3CCONH\}_2C_6H_2)_2]^{2-}$: m/z 1103.8. Found: 1103.5. Absorption spectrum (DMF): λ_{max} (ε, M^{-1} cm^{-1}) 348 (sh) (10 000), 412 (920), 452 (sh) (590) nm. Absorption spectrum (toluene): λ_{max} (ε, M^{-1} cm^{-1}) 337 (sh) (11 000), 395 (1000), 455 (sh) (550) nm. Anal. Calcd for $C_{156}H_{204}N_6O_5S_4Mo$: C, 75.93; H, 8.33; N, 3.41. Found: C, 74.91; H, 8.35; N, 3.43.

The disagreement with elemental analysis results for molybdenum complexes is probably caused by their nanoporous structure in the solid state (crystallographic data†). After removing the solvent molecules from the crystals, the resulting voids might be able to trap gaseous water molecules. Formal addition of water to the chemical formula improved the results. The calculated values for $C_{156}H_{204}N_6O_5S_4Mo\cdot(H_2O)_{1.8}$: C, 74.95; H, 8.37; N, 3.36, which agree with the found ones. The water molecules were also detected in ^{1}H NMR spectra, but the amount of water depended on the reaction conditions. Similar results were also found for **1-W**, **2-Mo**, and **2-W**.

$(Et_4N)_2[W^{IV}O(1,2\text{-}S_2\text{-}3,6\text{-}\{(4\text{-}^tBuC_6H_4)_3CCONH\}_2C_6H_2)_2]$ (1-W)

A suspension of **L1** (1.01 g, 0.936 mmol) and Et_4NBH_4 (1.42 g, 9.81 mmol) in a mixture of acetonitrile (53 mL) and water (2 mL) was refluxed at 70 °C for 3 h to afford a greenish-yellow solution and a colorless precipitate. The supernatant was separated, and a solution of $(Et_4N)[W^VO(SPh)_4]$ (288 mg, 0.375 mmol) in acetonitrile (25 mL) was added dropwise to the solution to afford a yellowish-white precipitate. The reaction mixture was stirred for 15 h at room temperature to afford a yellow solution and a yellowish-white precipitate. The supernatant was removed, and the precipitate was washed several times with acetonitrile using centrifugation. The product was extracted with toluene and concentrated to dryness to afford a yellow powder. The crude product was recrystallized from toluene–acetonitrile to afford yellowish-orange blocks. Yield: 252 mg, 28%. ^{1}H NMR (toluene-d_8): δ 8.94 (s, 4H, NH), 8.20 (s, 4H, 4,5-H), 7.69 (d, J = 8.5 Hz, 24H, Ar), 7.37 (d, J = 8.5 Hz, 24H, Ar), 1.86 (br, 16H, Et_4N^+), 1.31 (s, 108H, ^{t}Bu), 0.35 (br, 24H, Et_4N^+). ^{1}H NMR (DMF-d_7): δ 9.11 (s, 4H, NH), 8.01 (s, 4H, 4,5-H), 7.44 (d, J = 8.7 Hz, 24H, Ar), 7.39 (d, J = 8.7 Hz, 24H, Ar), 3.34 (q, J = 7.3 Hz, 16H, Et_4N^+), 1.26 (s, 108H, ^{t}Bu), 1.26 (tt, J_{H-H} = 7.3 Hz, J_{H-N} = 1.8 Hz, 24H, Et_4N^+). Absorption spectrum (toluene): λ_{max} (ε, M^{-1} cm^{-1}) 342 (sh) (9100), 425 (sh) (1300) nm. Anal. Calcd for $C_{156}H_{204}N_6O_5S_4W\cdot CH_3CN\cdot(H_2O)_{1.6}$: C, 72.28; H, 8.07; N, 3.73. Found: C, 72.27; H, 7.95; N, 3.93.

$(Et_4N)_2[Mo^{VI}O_2(1,2\text{-}S_2\text{-}3,6\text{-}\{(4\text{-}^tBuC_6H_4)_3CCONH\}_2C_6H_2)_2]$ (2-Mo)

A solution of Me_3NO (0.42 mg, 5.6 μmol) in DMF (0.2 mL) was added to a solution of **1-Mo** (6.8 mg, 2.8 μmol) in DMF (1.2 mL). The solution immediately turned reddish-purple. After removing the solvent under reduced pressure, the reddish-purple residue was extracted with toluene. The solution was concentrated to dryness under reduced pressure, and the resulting reddish-purple solid was recrystallized from acetonitrile to afford dark brown blocks. Yield: 4.0 mg, 58%. ^{1}H NMR (CD_3CN): δ 8.49 (s, 4H, NH), 7.73 (s, 4H, 4,5-H), 7.33 (d, J = 8.7 Hz, 24H, Ar), 7.23 (d, J = 8.7 Hz, 24H, Ar), 3.04 (q, J = 7.3 Hz, 16H, Et_4N^+), 1.24 (s, 108H, ^{t}Bu), 1.12 (tt, J_{H-H} = 7.3 Hz, J_{H-N} = 1.9 Hz, 24H, Et_4N^+). ESI-MS (CH_3CN, M^{2-} = $[Mo^{VI}O_2(1,2\text{-}S_2\text{-}3,6\text{-}\{(4\text{-}^tBuC_6H_4)_3CCONH\}_2C_6H_2)_2]^{2-}$) calcd for M^{2-}: m/z 1111.2. Found: 1111.5. Absorption spectrum (DMF): λ_{max} (ε, M^{-1} cm^{-1}) 364 (10 000), 398 (sh) (7500), 531 (2100) nm. Absorption spectrum (toluene): λ_{max} (ε, M^{-1} cm^{-1}) 357 (12 000), 392 (sh) (7800), 548 (2300) nm. Anal. Calcd for $C_{156}H_{204}N_6O_6S_4Mo\cdot(H_2O)_3$: C, 73.84; H, 8.34; N, 3.31. Found: C, 73.82; H, 8.15; N, 3.32.

$(Et_4N)_2[W^{VI}O_2(1,2\text{-}S_2\text{-}3,6\text{-}\{(4\text{-}^tBuC_6H_4)_3CCONH\}_2C_6H_2)_2]$ (2-W)

To a mixture of **1-W** (131.7 mg, 51.5 μmol) and Me_3NO (8.74 mg, 116 μmol) was added DMF (5 mL), and the mixture was stirred for 2 h to afford a reddish-orange solution. After removing the solvent under reduced pressure, the reddish-orange residue was extracted with toluene. The solution was concentrated to dryness under reduced pressure, and the resulting reddish-orange solid was recrystallized from acetonitrile to afford reddish-orange blocks. Yield: 100.7 mg, 76%. ^{1}H NMR (CD_3CN): δ 8.44 (br, 4H, NH), 7.73 (s, 4H, 4,5-H), 7.34 (d, J = 8.2 Hz, 24H, Ar), 7.23 (d, J = 8.2 Hz, 24H, Ar), 3.10 (q, J = 7.2 Hz, 16H, Et_4N^+), 1.24 (br, 108H, ^{t}Bu), 1.16 (tt, J_{H-H} = 7.2 Hz, J_{H-N} = 1.9 Hz, 24H, Et_4N^+). ESI-MS (CH_3CN, M^{2-} = $[W^{VI}O_2(1,2\text{-}S_2\text{-}3,6\text{-}\{(4\text{-}^tBuC_6H_4)_3CCONH\}_2C_6H_2)_2]^{2-}$) calcd for M^{2-}: m/z 1155.1. Found: 1155.7. IR (Nujol): 3316 (ν_{NH}), 1671 ($\nu_{C=O}$) cm^{-1}. Absorption spectrum (toluene): λ_{max} (ε, M^{-1} cm^{-1}) 360 (sh) (9200), 436 (2100), 495 (840) nm. Anal. Calcd for $C_{156}H_{204}N_6O_6S_4W\cdot H_2O$: C, 72.36; H, 8.02; N, 3.25. Found: C, 72.34; H, 7.93; N, 3.36.

Physical measurements

The elemental analyses were performed on a Yanaco CHN CORDER MT-5. ^{1}H NMR spectra were obtained with JEOL ECA-500, GSX-400, and ECS-400 spectrometers in chloroform-d, dichloromethane-d_2, acetonitrile-d_3, *N*,*N*-dimethylformamide-d_7, or toluene-d_8 at 303 K. Totally correlated spectroscopy (TOCSY) and rotating frame Overhauser enhancement (ROE) and exchange spectroscopy (ROESY) spectra were recorded on a VARIAN VNS-600 spectrometer in toluene-d_8 at 228 K with a mixing time of 500 ms. Electrospray ionization mass spectroscopy (ESI-MS) measurements were performed on a Finnigan MAT LCQ ion trap mass spectrometer using an acetonitrile solution. UV-visible absorption spectra were

recorded using a SHIMADZU UV-3100PC spectrometer. Infrared (IR) spectroscopic measurements were done on a Jasco FT/IR-4000 spectrometer. Raman spectra were measured at 298 K on a Jasco NR-1800 spectrophotometer with a liq. N_2 cooled CCD detector. Exciting radiation was provided by an Ar^+ ion laser (514.5 nm). The measurements of cyclic voltammograms (CVs) in a DMF solution were carried out on a BAS 100B/W instrument with a three-electrode system: a glassy carbon working electrode, a Pt-wire auxiliary electrode, and a saturated calomel electrode (SCE). The scan rate was 100 mV s^{-1}. The concentration of the sample was 2.5 mM, containing 0.1 M of $^nBu_4NClO_4$ as a supporting electrolyte. The result was cross-referenced using the ferrocene/ferrocenium couple as a calibrant. The redox potential of ferrocene/ferrocenium was observed at +0.48 V *vs.* SCE under the same conditions.

Kinetic measurements

A reaction system containing **1-Mo** and Me_3NO was monitored spectrophotometrically in the range 280–800 nm. The measurements were carried out in a 1 cm UV cell containing a solution of **1-Mo** (0.1 mM, 3.0 mL) at 27 °C (solvents: DMF, THF, toluene). After thermal equilibrium, a Me_3NO solution (60 mM, 10 μL) in DMF was injected through a silicone rubber cap, and the cell contents were quickly mixed by shaking. The time course of the reaction was monitored using the absorption maximum of **2-Mo**. All calculations for the data analysis were performed at 531, 537, and 548 nm in DMF, THF, and toluene, respectively.

Results

Synthesis of the ligand

In the process of searching for a precursor of the dithiolate ligand that contained bulky triarylmethyl CAr_3 substituents, a benzotrithiol derivative, 1,2-S_3-3,6-$\{(4\text{-}^t BuC_6H_4)_3CCONH\}_2C_6H_2$ (**L1**), with a trisulfide bond was found and isolated. To synthesize a diaryl disulfide compound, Bunte salts are generally used as the protecting group for thiophenol derivatives. We previously synthesized a disulfide derivative with bulky CPh_3 substituents $\{1,2\text{-}S_2\text{-}3,6\text{-}(Ph_3CCONH)_2C_6H_2\}_2$ by deprotecting the corresponding Bunte salt using alkanethiolate in methanol and air oxidation.[23] At first, deprotection of the Bunte salt with bulky hydrophobic substituents, $(^nBu_4N)_2[3,6\text{-}\{(4\text{-}^tBuC_6H_4)_3\text{-}CCONH\}_2C_6H_2\text{-}1,2\text{-}(SSO_3)_2]$, was attempted using EtSNa by a previously reported procedure. However, the reaction hardly proceeded because of the steric hindrance and the lack of reactant solubility in methanol, and only a small amount of an asymmetric disulfide, 3,6-$\{(4\text{-}^tBuC_6H_4)_3CCONH\}_2C_6H_2\text{-}1,2\text{-}(SSEt)_2$, was obtained. Another method for deprotecting Bunte salts using thiourea[40] gave a benzotrithiol derivative, **L1**, as yellow blocks which were isolated in a 56% yield (Scheme 1). **L1** was characterized by X-ray structural analysis, ^1H NMR, IR, and elemental analysis (Fig. S1,† Table S1†). Its unexpected structure can be explained by the steric hindrance on the sulfur atoms of a thiourea-bound intermediate, which prefers an intramolecular cyclization reaction to the intermolecular formation of two disulfide bonds (Scheme S1†). We used **L1** as a precursor for the desired ligand because **L1** is chemically and thermodynamically stable and reducible by borohydride to afford the desired dithiolate ligand.

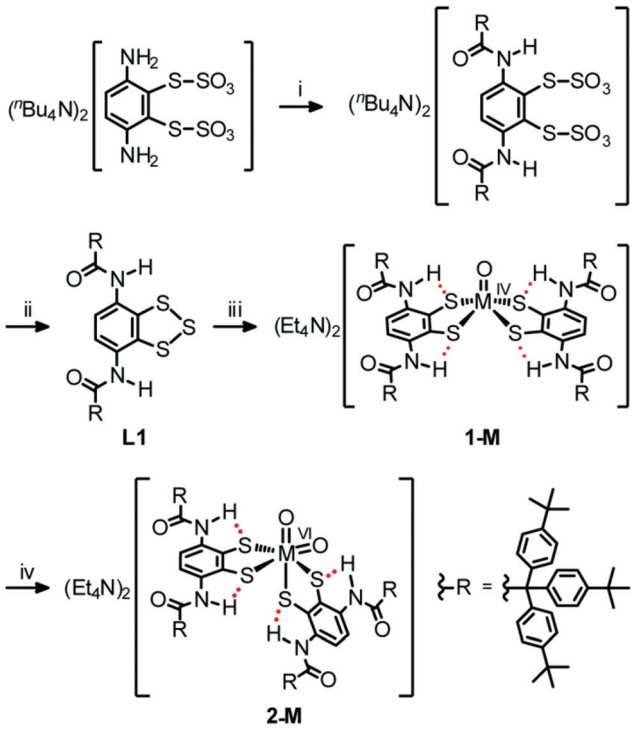

Scheme 1 (i) RCOCl, Et_3N, 96%. (ii) $(NH_2)_2CS$/AcOH, 56%. (iii) Et_4NBH_4, then $(Et_4N)[M^VO(SPh)_4]/CH_3CN/H_2O$, 48%(Mo), 28%(W). (iv) Me_3NO/DMF, 58%(Mo), 76%(W).

Synthesis of the complexes

Monooxo-molybdenum(IV) and tungsten(IV) complexes, $(Et_4N)_2[M^{IV}O(1,2\text{-}S_2\text{-}3,6\text{-}\{(4\text{-}^tBuC_6H_4)_3CCONH\}_2C_6H_2)_2]$ (**1-M**, M = Mo, W), were obtained using the reactions shown in Scheme 1. These complexes were synthesized by a method similar to that previously reported.[23,24,27] A ligand-exchange reaction in acetonitrile was carried out between the dithiolate ligand, prepared by reduction of **L1** with excess Et_4NBH_4, and a M^V starting complex, $(Et_4N)[M^VO(SPh)_4]$ (M = Mo, W). The subsequent reduction of the M^V species by residual borohydride anions gave **1-M** as a yellowish-white precipitate. Since the **1-M** complexes have negligible solubility in acetonitrile, the precipitate was thoroughly washed with acetonitrile and selectively extracted with toluene. The pure molybdenum(IV) complex, **1-Mo**, was isolated as yellow blocks *via* recrystallization from toluene in a 48% yield, and the recrystallization of the tungsten(IV) complex, **1-W**, from a mixture of toluene and acetonitrile resulted in orange blocks in a 28% yield.

Dioxo-molybdenum(VI) and tungsten(VI) complexes, $(Et_4N)_2\text{-}[M^{VI}O_2(1,2\text{-}S_2\text{-}3,6\text{-}\{(4\text{-}^tBuC_6H_4)_3CCONH\}_2C_6H_2)_2]$ (**2-M**, M = Mo, W), were obtained by the oxygen-atom-transfer (OAT) reaction between the corresponding complexes, **1-M** and Me_3NO

(Scheme 1). The reaction proceeded immediately in DMF at room temperature. The pure molybdenum(VI) complex, **2-Mo**, was isolated as dark brown blocks by recrystallization from acetonitrile in a 58% yield, and the tungsten derivative, **2-W**, was isolated as reddish-orange blocks from acetonitrile in a 76% yield. The dioxomolybdenum(VI) complex **2-Mo** is quite stable in both the solid and solution states compared to other dioxomolybdenum(VI) complexes containing 3,6-bis(acylamino)benzene-1,2-dithiolate ligands, which are too unstable to be isolated.[23,24,27] The complex is considered to be thermodynamically stabilized by its bulky substituents and NH···π hydrogen bonds between amide NH and the adjacent CAr_3 group, which weaken the NH···S hydrogen bond as described in the following section.

Molecular structures in the crystals

The molecular structures of **1-M** and **2-M** (M = Mo, W) were determined by X-ray analysis. These complexes were apparently recrystallized easily but the crystallinity was very low like gel because of the highly-disordered structures inside the organic frameworks or capsules. Although careful recrystallization and selection of crystals were repeated, the quality of the data was quite poor, resulting in large *R* factors. Unfortunately, the structural details cannot be described; however, the rough structures and the packing must be correct. Here, we mainly discuss the relative location of counter cations and conformation of substituents. The preliminary structure of **2-Mo** was only used to confirm that **2-Mo** was isomorphous and isostructural to **2-W**. The details of the refinements are shown in ESI and crystallographic data.†

Two molecular structures of **1-Mo** were obtained and varied depending on the crystallization solvents. The molecular structure of **1-Mo**·8(toluene), obtained by crystallization from toluene, is shown in Fig. 1. Recrystallization of **1-Mo** from toluene–acetonitrile gave acetonitrile-containing blocks. The ORTEP drawing and illustrations of **1-Mo**·toluene·5CH_3CN are shown in Fig. S2.† The CAr_3 moieties are bulky enough to interlock with each other in the crystal, so the possible symmetries of the four CAr_3 moieties are C_2 and C_i. As shown in Fig. 2, the anion part of **1-Mo**·8(toluene) has a pseudo-C_i symmetry (the molecular structure showed a pseudo-center of symmetry, see CIF†), and the anion part of **1-Mo**·toluene·5CH_3CN has a C_2 symmetry. The crystal of **1-W**· 4(toluene)·3CH_3CN·H_2O is essentially isomorphous to that of **1-Mo**·toluene·5CH_3CN with similar cell parameters. The anion part is also C_2 symmetry (Table S2†). In this paper, we discuss the molecular structure of **1-Mo**·8(toluene) because it is the highest quality crystal.

The Mo center of **1-Mo**·8(toluene) shows a square pyramidal geometry similar to $(Et_4N)_2[Mo^{IV}O\{1,2\text{-}S_2\text{-}3,6\text{-}(CH_3CONH)_2\text{-}C_6H_2\}_2]$ (**3-Mo**, Chart 2). All of the amide NH moieties were directed toward the sulfur atoms of the dithiolate ligand, which indicated the presence of NH···S hydrogen bonds. The aromatic ring of the substituent is close to the NH group suggesting the formation of an NH···π hydrogen bond.[41] Bifurcated (NH···S and NH···π) hydrogen bonds are known[42] and

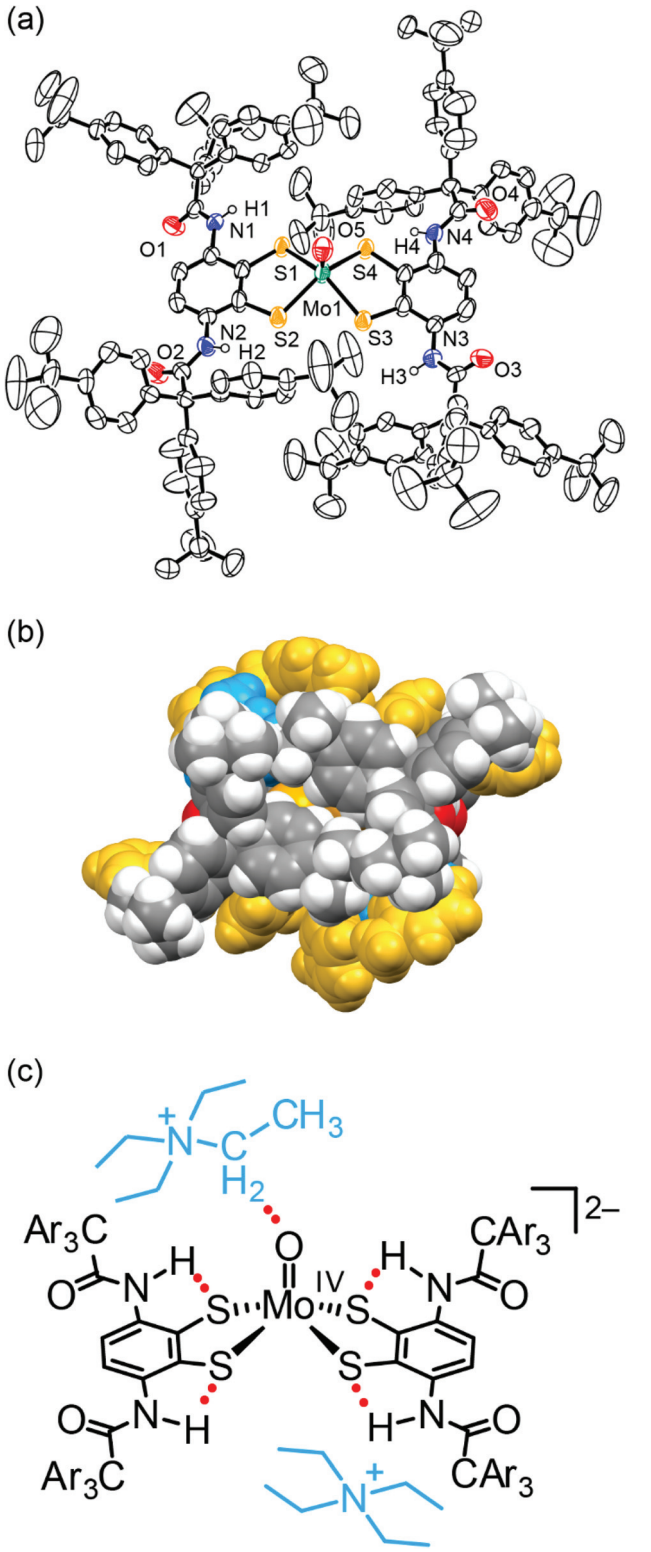

Fig. 1 (a) ORTEP drawing of **1-Mo**·8(toluene) at 50% probability (anion part, protons are omitted for clarity except amide groups) and (b) space-filling model with Et_4N^+ (blue) and toluene (yellow). (c) Schematic drawing of the interionic CH···O═Mo interaction in the crystal.

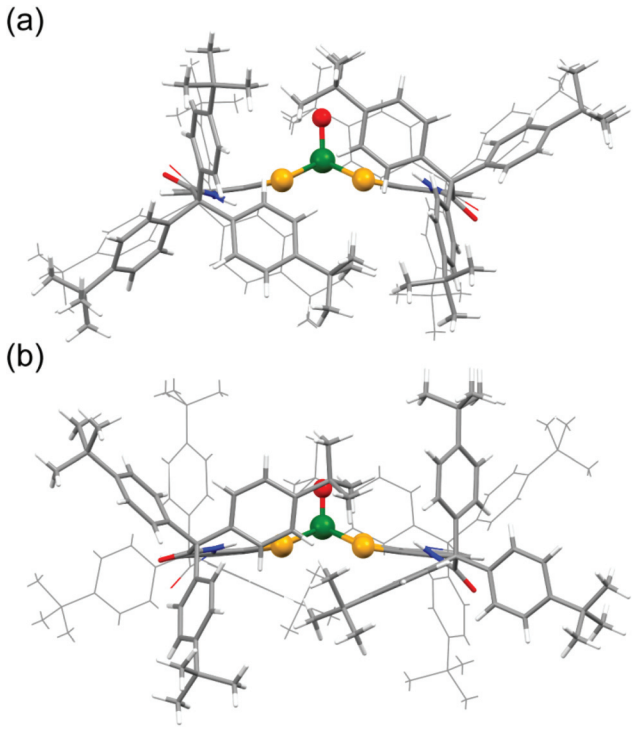

Fig. 2 Side-view structures of the anion part of (a) **1-Mo**·8(toluene) and (b) **1-Mo**·toluene·5CH_3CN.

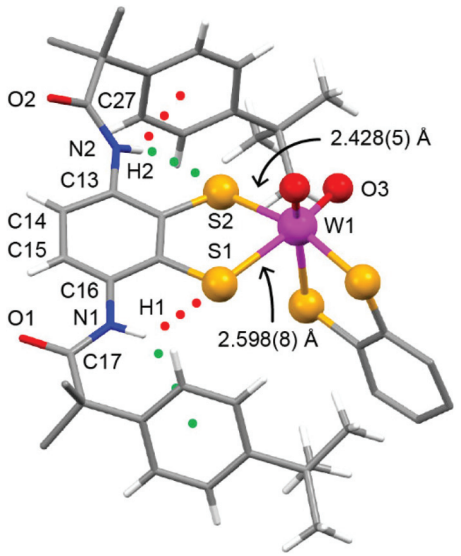

Fig. 3 A simplified molecular structure of the anion part of **2-W**·5CH_3CN. Four 4-^{t}BuC_6H_4 moieties and two of the acylamino groups were omitted for clarity.

can perturb the strength of the N–H bond. The change was not detected by structural analysis but was found in the IR spectra described later. One of the two Et_4N^+ counterions was found close to the terminal oxo ligand suggesting the formation of a CH···O=Mo interaction (Fig. 1c). Similar interactions between an oxo ligand and counter cations have been reported.[43–46] In the space-filling model of **1-Mo**·8(toluene) (Fig. 1b), the polar MoO moiety and Et_4N^+ counterions (blue) are covered by the walls formed by the bulky hydrophobic ligands. These ligand walls can prevent intermolecular ionic interactions, and this makes the complex soluble in nonpolar solvents like toluene.

The W center of **2-W**·5CH_3CN shows a slightly distorted octahedral geometry similar to $(Et_4N)_2[W^{VI}O_2\{1,2\text{-}S_2\text{-}3,6\text{-}(CH_3CONH)_2C_6H_2\}_2]$ (**4-W**). The molecular structure of **2-W**·5CH_3CN is shown in Fig. S3.† The crystals of **2-Mo**·5CH_3CN and **2-W**·5CH_3CN are isomorphous (Table S2†). The two dithiolate ligands are crystallographically equivalent owing to the C_2 axial symmetry across the bisector of the O–W–O angle. Two Et_4N^+ counterions were found close to the terminal oxo ligands with CH···O=W interactions (Fig. S3c†).

As shown in Fig. 3 and Table S3,† the geometrical parameters of **2-W** were similar to the reported values of **4-W**, showing the longer W–S at the position *trans* to W=O owing to a strong *trans* influence of the oxo ligand and the unsymmetrical structure with the stronger (red) and the weaker (green) NH···S hydrogen bonds. The amide NH at the position *cis* to the oxo ligand is directed towards the benzene ring of the CAr_3 moiety rather than the sulfur atom suggesting the presence of an NH···π hydrogen bond. The NH···π hydrogen bond decreases the contribution of NH···S, resulting in an increase in donation from S to W. The W–S bond at the position *cis* to the oxo ligand is thought to be stabilized by the intermolecular NH···π hydrogen bond between the amide NH and benzene ring of the neighboring dithiolate ligand. On the other hand, an NH···π hydrogen bond is only seen in an intermolecular fashion in the crystal of **4-W**.

IR and Raman spectra

The presence of NH···S hydrogen bonds was confirmed by IR spectroscopy. IR data for **1-M** and **2-M** in the solid state are listed in Table 1 along with the values of the related complexes, $(Et_4N)_2[M^{IV}O\{1,2\text{-}S_2\text{-}3,6\text{-}(CH_3CONH)_2C_6H_2\}_2]$ (**3-M**) and $(Et_4N)_2[W^{VI}O_2\{1,2\text{-}S_2\text{-}3,6\text{-}(CH_3CONH)_2C_6H_2\}_2]$ (**4-W**). As described in a previous paper,[27] the strength of the hydrogen bond is evaluated using the negative shift of ν(NH) compared to the corresponding compound without a hydrogen bond. RCONHPh is used as a reference in this paper. The $\Delta\nu$(NH) values of **1-Mo** and **1-W** (−97 and −99 cm^{-1}, respectively) are

Table 1 IR bands of ν(NH) (cm^{-1}) in the molybdenum and tungsten complexes in the solid state

	Complexes[a]	Δ(NH)[b]
1-Mo	3306	−97
1-W	3304	−99
2-Mo	3307	−96
2-W	3316	−87
3-Mo[c]	3346	−85
3-W[d]	3346	−85
4-W[d]	3370, 3316	−61, −115

[a] Nujol. [b] Differences from the value (3403 cm^{-1} for **1-M** and **2-M**, 3431 cm^{-1} for **3-M** and **4-M**) of the corresponding compound, RCONHPh in solution (10 mM in CH_2Cl_2). [c] Ref. 23. [d] Ref. 24.

more negative than those of **3-Mo** and **3-W** (−85 and −85 cm^{-1}, respectively), which by conventional estimation indicates stronger hydrogen bonds in the complexes with bulky substituents. However, **1-M** forms bifurcated (NH···S and NH···π) hydrogen bonds and not the simple NH···S hydrogen bonds seen in **3-M**. In this case, it is necessary to take into account the contribution of the NH···π hydrogen bond. The NH···π hydrogen bond is favorably formed with a fixed orientation of the aromatic ring to the NH group seen in **1-M** and lowers ν(NH) significantly. The NH···π hydrogen bond is not as strongly formed in the reference compound, RCONHPh, compared to **1-M**. The conventional evaluation based on the obtained $\Delta\nu$(NH) for **1-M** must overestimate the strength of the NH···S hydrogen bond. Therefore, the net strength should be weaker. Moreover, the perturbation of the NH···π hydrogen bond likely weakens the competing NH···S hydrogen bond.

In IR spectra of **2-W**, a single but relatively broad band was observed even though the presence of two distinct hydrogen bonds was suggested in the crystal (Fig. S4†). On the other hand, **4-W**, with CH_3 substituents, exhibited two distinct ν(NH) bands (3370 and 3316 cm^{-1}) in the solid state. The ν(NH) at the position *cis* to the oxo ligand was observed at a wavenumber 54 cm^{-1} higher. The ν(NH) band at 3316 cm^{-1} of **2-W** can be fitted by a single Gaussian curve (Fig. S4b,† red dashed line) with a full width at half maximum (FWHM) of 66 cm^{-1}. The curve is reasonably separated into two equivalent Gaussian curves at 3326 and 3306 cm^{-1} (green lines). The difference of the two peaks is only 20 cm^{-1} smaller than the FWHM; therefore the stretching vibrations could not be detected as two bands. The results indicate that the relatively stronger NH bond at the *cis* position was significantly weakened by the formation of the NH···π hydrogen bond in **2-W** (see Fig. 3).

IR ν(MO) bands of **1-M** are listed in Table 2 along with those of the related complexes, **3-M** and $(Et_4N)_2[M^{IV}O(1,2\text{-}S_2C_6H_4)_2]$ (**7-M**) without the hydrogen bond.[47–49] The stabilization of the M^{IV}═O bonds of monooxo-molybdenum(IV) and tungsten(IV) complexes by NH···S hydrogen bonds was observed for **1-M**, as well as **3-M**. The results are consistent with the tendency of the NH···S hydrogen-bonded complexes described in previous papers.[23,27]

The symmetric and asymmetric MO_2 stretching bands of **2-Mo** and **2-W**, ascribed to the *cis*-dioxo configuration, were clearly observed by resonance Raman spectroscopy excited at 514.5 nm in the LMCT band (Fig. S5†). These values are listed in Table 3 together with the related compounds and the differences from $(Et_4N)_2[M^{VI}O_2(1,2\text{-}S_2C_6H_4)_2]$ (**8-M**) are shown in parentheses. Because a dioxomolybdenum(VI) complex with CH_3 substituents (**4-Mo**) was not isolated by thermodynamic instability,[23] only the values for **4-W** are shown.[24] The wavenumber shifts of **2-M** (23 and 21 cm^{-1}) were larger than those of **4-W** (14 cm^{-1}).

Table 2 IR bands of ν(MO) (cm^{-1}) in the monooxo-molybdenum(IV) and tungsten(IV) complexes in the solid state

	ν(MO)	$\Delta\nu$(MO)[a]
1-Mo	921	+16
1-W	920	+14
3-Mo[b]	922	+17
3-W[c]	912	+6
7-Mo[d]	905	
7-W[e]	906	

[a] Differences from the value of $(Et_4N)_2[M^{IV}O(1,2\text{-}S_2C_6H_4)_2]$ (**7-M**). [b] Ref. 23. [c] Ref. 24. [d] Ref. 47. [e] Ref. 49.

Table 3 Resonance Raman bands of $\nu(MO_2)$ (cm^{-1}) in the dioxomolybdenum(VI) and tungsten(VI) complexes in the solid state[a]

	Mo		W	
	$\nu_s(MoO_2)$	$\nu_{as}(MoO_2)$	$\nu_s(WO_2)$	$\nu_{as}(WO_2)$
2-M	881 (+23)	846 (+17)	906 (+21)	865 (+22)
4-M[b]			899 (+14)	854 (+11)
8-M[c]	858	829	885	843

[a] Differences from the value of $(Et_4N)_2[M^{VI}O_2(1,2\text{-}S_2C_6H_4)_2]$ (**8-M**) are shown in parentheses. [b] Ref. 23 and 24. [c] Ref. 34 and 49.

^{1}H NMR studies

^{1}H NMR spectra of the monooxo-molybdenum(IV) and tungsten(IV) complexes (**1-M**) are shown in Fig. 4. Because the **1-M** complexes are only slightly soluble in acetonitrile, the ^{1}H NMR measurements were carried out in DMF-d_7 (Fig. 4a and c) and toluene-d_8 (Fig. 4b and d). **1-M** exhibited well defined signals in DMF-d_7 as did the related molybdenum(IV) complexes in CD_3CN,[25–27] but some crystal solvent peaks (labeled by asterisks) were observed. On the other hand, the broadened and upfield-shifted signals of the Et_4N^+ counterions, **e** and **g**, were observed in toluene-d_8. These results probably arose from shielding by the benzene rings of the ligand. In the crystal of **1-M**, the Et_4N^+ counterions are located at a position shielded by the benzene rings of the dithiolate ligand and CAr_3 groups. Though the shielding effect depends on the spatial position and direction, only a single set of signals was observed because the molecular motion was faster than the NMR timescale. Upon cooling to 228 K, the signals of Et_4N^+ broadened and the signal **g** split into two distinct signals (Fig. S6†). The result can be explained by a decrease in the molecular motion, resulting in the construction of two distinct environments by shielding of the MoO moiety, which has a triple bond character (formally expressed as Mo≡O^+)[50] and whose effect was the stronger the closer the Et_4N^+ counterion is to the oxo ligand (upper side of Fig. 1c).

The ^{1}H NMR spectrum of **2-W** showed a single set of broad signals in a polar solvent, CD_3CN, although the green and red protons of one ligand are essentially nonequivalent in the *cis*-dioxo octahedral configuration but two ligands are equivalent in C_2-symmetric molecular structures (Fig. 5). The observation is caused by fast conformational changes, which are relatively slow in the nonpolar solvent, toluene-d_8 (Fig. 5b). Upon cooling to 228 K in toluene-d_8, the signals sharpened and a pair of signals separated into two sets of signals (Fig. 5c).

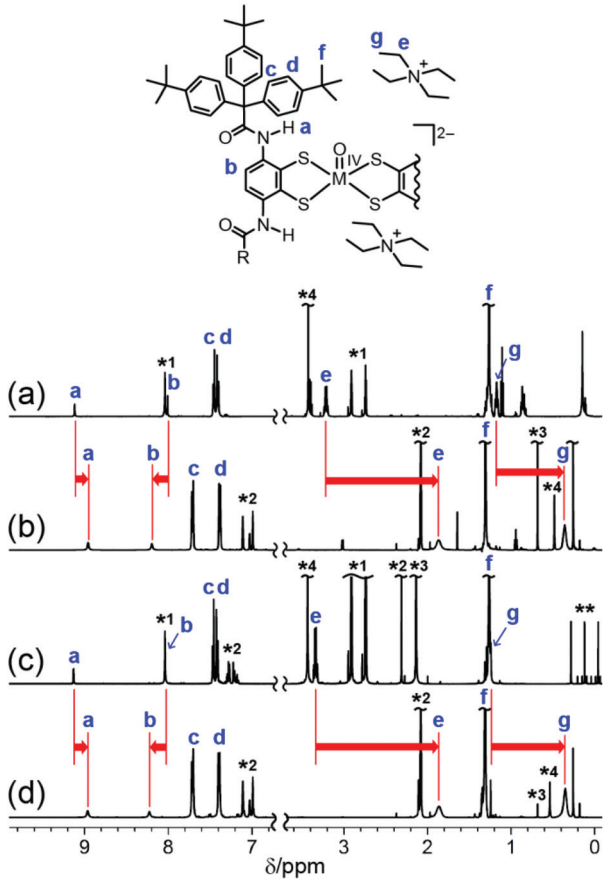

Fig. 4 ^{1}H NMR spectra of (a) **1-Mo** in DMF-d_7, (b) **1-Mo** in toluene-d_8, (c) **1-W** in DMF-d_7, and (d) **1-W** in toluene-d_8 at 303 K. The asterisks denote solvents as a contaminant (*1: DMF; *2: toluene; *3: acetonitrile; *4: water). The double asterisk (**) denotes BH_4^- used for the clear spectrum by reducing a trace amount of $W^{V}O$ species.

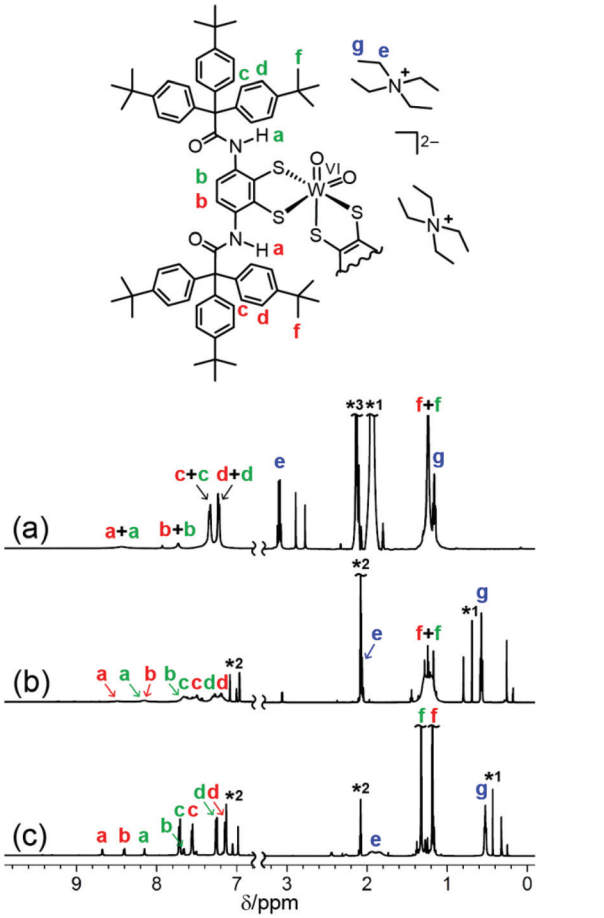

Fig. 5 ^{1}H NMR spectra of **2-W** in (a) CD_3CN at 303 K, (b) toluene-d_8 at 303 K, and (c) toluene-d_8 at 228 K. The asterisks denote solvents as a contaminant (*1: acetonitrile; *2: toluene; *3: water).

Because the NH proton forming the stronger NH···S hydrogen bond is observed at the lower field[27] and the NH···S at the position *trans* to the oxo ligand is stronger than *cis*,[24] the lowest signal is reasonably assigned to the NH proton at the position *trans* to the oxo ligand. Therefore the other signals were assigned to each side of the ligand at the positions *trans* (red) and *cis* (green) to the oxo ligand using TOCSY and ROESY spectra (Fig. S7†). The rotating frame Overhauser effects (ROE) between red **f** and green **a**, **b** were observed indicating the fixed conformation, but were absent between green **f** and red **a** in ROESY spectra, which are in accord with the molecular structure in the crystal. These observations prove the validity of the assignments. In addition, the interionic ROE was observed between signals **b** and **g**, which is consistent with the relative location of Et_4N^+ in the crystal.

Variable temperature (VT) NMR analysis of **2-W** confirmed that the signals separated in various solvents at low temperature. Thermodynamic parameters of the chemical exchange estimated from VT NMR spectra using line shape analysis are summarized in Table 4. The Eyring plot in various solvents gave $\Delta H^{\ddagger}$, $\Delta S^{\ddagger}$, and $\Delta G^{\ddagger}$. The activation free energies, $\Delta G^{\ddagger}$, were estimated to be 58.1–64.1 kJ mol^{-1} which are larger than

Table 4 Thermodynamic parameters of **2-W** in various solvents

Solvent	ε_r [a]	$\Delta H^{\ddagger}$/ kJ mol^{-1}	$\Delta S^{\ddagger}$/ J K^{-1} mol^{-1}	$\Delta G^{\ddagger}$ [b]/ kJ mol^{-1}
CD_3CN	35.9	43.4	−48.7	58.1
DMF-d_7	36.7	59.5	−5.6	61.1
CD_2Cl_2	8.93	53.9	−33.8	64.1
Toluene-d_8	2.38	51.9	−39.0	63.7
Toluene-d_8 [c]	2.38	47.1	−26.6	55.1

[a] Ref. 55. [b] Calculated from the formula $\Delta G^{\ddagger} = \Delta H^{\ddagger} - T\Delta S^{\ddagger}$ at 303 K. [c] **2-Mo**.

that ($\Delta G^{\ddagger}$ = 43.2 kJ mol^{-1}) of the related complex without hydrogen bonds, $(Et_4N)_2[W^{VI}O_2(1,2\text{-}S_2\text{-}3,6\text{-}Cl_2C_6H_2)_2]$ in THF-d_8.[51] The activation entropies, $\Delta S^{\ddagger}$, were negative in all cases, which indicates that the conformational change proceeds through a Bailar twist mechanism without dissociation of the ligands as shown in Fig. 6, where two enantiomers are identical in NMR spectroscopy.[52–54] The bulky substituents are expected to restrict the possible conformations, which enlarges the negative entropy of activation. In addition, the activation

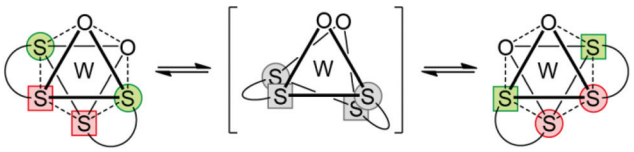

Fig. 6 Proposed mechanism of the conformational change of **2-W** in solution. The square and the circle represent two different environments. The color of squares and circles corresponds to the assignment of ^{1}H NMR signals.

enthalpies, $\Delta H^{\ddagger}$, were relatively large in nonpolar solvents, which allowed observation of the green and red protons in Fig. 5 even at room temperature. The small entropy of activation in DMF with a large donor number suggests the presence of a dissociative isomerization mechanism. VT NMR analysis of **2-Mo** in toluene-d_8 gave a relatively small activation free energy ($\Delta G^{\ddagger}$ = 55.1 kJ mol^{-1}) compared to **2-W**. In the case of **2-Mo**, two distinct signals were not observed in toluene-d_8 at room temperature owing to the fast conformational change, which was probably caused by the lability of the Mo–S bonds.

Electrochemical properties

The redox potentials of **1-M** in DMF are listed in Table 5 along with those of **3-M** with CH_3 substituents and **7-M** without hydrogen bonds. The cyclic voltammogram of **1-M** exhibits a reversible Mo(IV)/Mo(V) redox couple at $E_{1/2}$ = −0.20 V *vs.* SCE and W(IV)/W(V) at −0.40 V, respectively. The redox potentials of **1-M** are 0.15 V and 0.23 V more positive than those of the corresponding **7-M**, which lacks NH···S hydrogen bonds. This is a common tendency for the molybdenum(IV) and tungsten(IV) complexes with NH···S hydrogen bonds. The redox potential of **1-M** is less positive than that of **3-M**, which has methyl groups. As described in the section "IR and Raman spectra", the evaluation of the strength of the NH···S hydrogen bond in **1-M** is difficult because of the significant contribution of the NH···π hydrogen bond. The less positive shift is explained by two reasons. One is that the NH···π hydrogen bond weakened the NH···S hydrogen bond of **1-M**, even though the total contribution of the NH···S and NH···π hydrogen bonds was larger than that of **3-M**. The other is the hydrophobic microenvironment formed by the bulky ligands reported in experimental[56,57] and theoretical[58] examinations on iron–sulfur proteins.

Table 5 Redox potentials of monooxo-molybdenum(IV) and tungsten(IV) complexes

	Mo		W	
	$E_{1/2}$	$\Delta E_{1/2}$ [a]	$E_{1/2}$	$\Delta E_{1/2}$ [a]
1-M	−0.20	+0.15	−0.40	+0.23
3-M[b]	−0.13	+0.22	−0.34	+0.29
7-M[c]	−0.35	—	−0.63	—

[a] Differences from the value of $(Et_4N)_2[M^{IV}O(1,2\text{-}S_2C_6H_4)_2]$ (**7-M**). [b] Ref. 23 and 24. [c] Ref. 47 and 49.

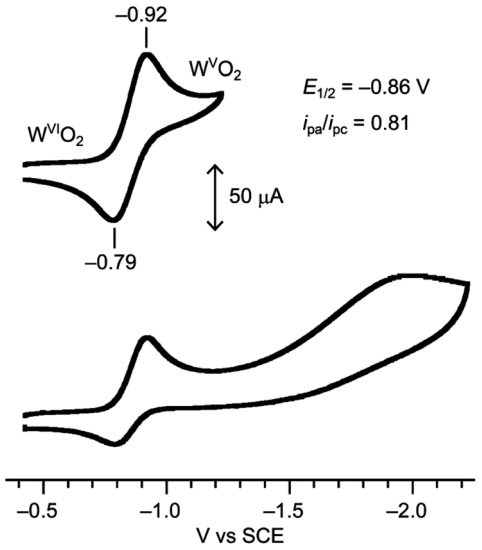

Fig. 7 Cyclic voltammogram of **2-W** in DMF scanning from −0.4 to −1.2 V (upper) and from −0.4 to −2.2 V (lower).

Complex **2-W** exhibits a pseudo-reversible W(VI)/W(V) redox couple at $E_{1/2}$ = −0.86 V *vs.* SCE (Fig. 7). As shown in previous reports, the redox couples of the dioxotungsten(VI) complexes with unsubstituted benzene-1,2-dithiolate ligands (**8-W**) and with 3,6-bis(acetylamino)benzene-1,2-dithiolate ligands (**4-W**) were irreversible because of the instability of the one electron reduced W^{V}O$_2$ species.[24,48,49] The electron-rich W^{V}O$_2$ species is thought to degrade *via* O-atom releasing reactions.[49,51,59] Improved reversibility was observed for $(Et_4N)_2[W^{VI}O_2\{1,2\text{-}S_2\text{-}3,6\text{-}(^t\text{BuCONH})_2C_6H_2\}_2]$, which contains relatively bulky ^{t}Bu groups. The explanation for this was that the ^{t}Bu groups prevented intermolecular reactions.[24] In the case of **2-W** with bulky hydrophobic CAr_3 groups, the reversibility was improved i_{pa}/i_{pc} = 0.81 but quantitative evaluation of the reversibility was difficult because of the successive irreversible redox process. The i_{pa}/i_{pc} value is the highest of the *cis*-dioxotetrathiolatotungsten(VI) complexes ($[W^{VI}O_2(SR)_4]^{2-}$) previously reported.[24,48,49,51,60] The reduction potential (E_p = −0.92 V) of **2-W** is positively shifted compared to −1.26 V of **8-W**, which lacks NH···S hydrogen bonds, and is negatively shifted compared to −0.82 V of **4-W** with CH_3 groups, and this is thought to be the effect of NH···S and NH···π hydrogen bonds and/or the hydrophobic microenvironment described for **1-M**. Unfortunately, **2-Mo** did not give well-defined Mo(VI)/Mo(V) redox couple although **2-Mo** is significantly stable compared to **4-Mo**.

Absorption spectra and reactivity

The UV-vis spectra of **1-Mo** and **2-Mo** in DMF are shown in Fig. 8. The spectrum of **1-Mo** shows absorption bands at 348, 412, and 452 nm and is similar to **5-Mo** with CPh_3 groups (348, 406, and 457 nm).[23] The spectrum of **2-Mo** shows absorption bands at 364, 398, and 531 nm, and the lowest transition energy assigned to the LMCT band (531 nm) was equal to that of **6-Mo**.[23] Upon addition of 2 eq. of Me_3NO to **1-Mo**, a rapid

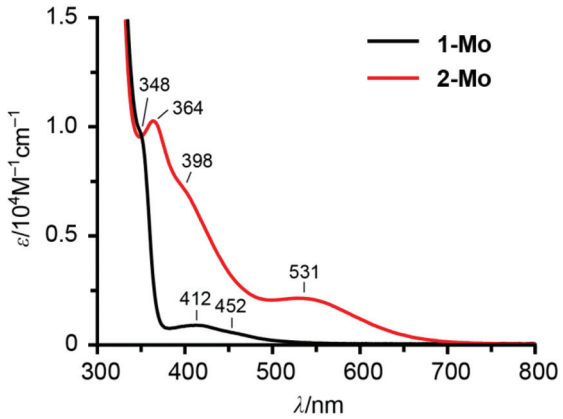

Fig. 8 UV-vis spectra of **1-Mo** (black) and **2-Mo** (red) in DMF.

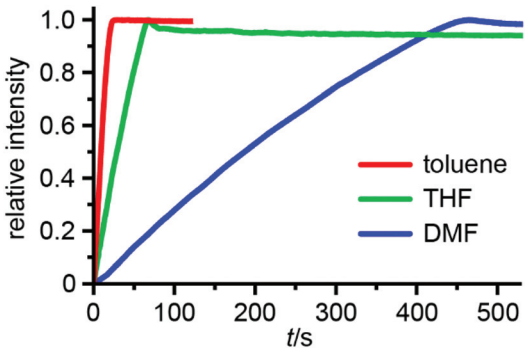

Fig. 9 Time course of the relative intensity of the absorption maximum of **2-Mo** in toluene (red), THF (green), and DMF (blue).

Table 6 Kinetic parameters of the reaction of **1-Mo** with Me_3NO in various solvents

Solvent	ε_r [a]	$k_2/M^{-1}\ s^{-1}$
DMF	36.7	26.6 ± 12.2
THF	7.58	106 ± 10
Toluene	2.38	384 ± 51

[a] Ref. 55.

oxygen-atom-transfer reaction proceeded to afford **2-Mo**. The reaction was monitored by examining the absorption maximum of **2-Mo** at 531 nm in DMF. The second-order rate constant of **1-Mo** in DMF (k_2 = 27 ± 12 $M^{-1}\ s^{-1}$) was comparable to the estimated k_2 ($k_{obs}/[\mathbf{5\text{-}Mo}]_0$ = 26 ± 0.1 $M^{-1}\ s^{-1}$) of **5-Mo** from the reported pseudo-first-order rate constant, k_{obs},[23] which indicates that the reaction proceeds *via cis*-attack of Me_3NO, as well as **5-Mo**.[23,27] In the case of **1-W**, the OAT reaction is too fast to evaluate the exact rate constant using our instruments, but at least approximately three times faster than **1-Mo**. This result indicates a similar tendency to previous studies.[24]

Surprisingly, in the nonpolar solvent (toluene) the reduction of Me_3NO proceeded about ten times faster than in DMF. In a medium polarity solvent, THF, the complex exhibited moderate reactivity (Fig. 9). The calculated k_2 values under these conditions are listed in Table 6 with the dielectric constant of the solvents, ε_r.[55] The results indicate that the substrate can easily approach the active center and efficiently interact with the complex in the hydrophobic environment, which supports attracting interactions between polar molecules.

Discussion

The molybdenum(IV, VI) and tungsten(IV, VI) complexes with NH···S hydrogen bonded hydrophobic benzene-1,2-dithiolate ligands are soluble in nonpolar solvents like toluene. The solubility allows a precise discussion about the solution structure and reactivity in various solvents. Here, we discuss the weak interactions in a hydrophobic environment and the effect of the triarylmethyl groups, in conjunction with their relevance to the nature of the molybdoenzyme.

Weak interactions in a hydrophobic environment

The **1-M** complexes with hydrophobic substituents are soluble in nonpolar solvents like toluene, allowing the observation of weak interionic interactions. Both of the solid state structures of **1-Mo** with different crystal solvents show interionic CH···O=Mo interactions, even though the configuration of four bulky CAr_3 groups is different. Generally such interactions cannot be observed in polar solvents because each ion is completely solvated. However, the ^1H NMR spectra in toluene-d_8 clearly showed the nonequivalent Et_4N^+ cations and proximity of the cation to the terminal oxo ligand.

The results correspond with the *cis*-attack of Me_3NO on the $Mo^{IV}O$ moiety in the reported mechanism.[23,25] In the attack of polar Me_3NO, the positively charged Me_3N moiety tended to be drawn by the basic terminal oxo ligand based on theoretical calculations.[27] Such interactions should be stabilized in nonpolar solvents and result in the acceleration of the reduction of Me_3NO, which is consistent with the experimental results for the reactivity of **1-Mo**.

A hydrophobic environment around the active site is a key factor for the activity of the enzymes involving substrate uptake and stabilization of transition states. In the latter case, Warshel proposed that enzymes can be considered as "supersolvents" that stabilize (solvate) ionic transition states by using noncovalent interactions more effectively than do aqueous solutions.[61] Experimentally, the artificial enzyme with a hydrophobic chain showed much large k_{cat} for catalytic transamination of pyruvic acid.[62]

On the basis of the X-ray structure of DMSOR, the presence of hydrogen bonds from the amino acid residues to the coordinated atoms at the base of the substrate access funnel has been proposed.[7,9,63–65] The mutation study revealed that an OH···O–Mo hydrogen bond between tyrosine 114 and the oxygen atom of the coordinated DMSO increases the affinity of the substrate for the metal center and the rate of the catalytic reaction.[64] Tryptophan 116 is thought to form an NH···O=Mo

hydrogen bond between the oxo ligand of the oxidized enzyme, which stabilizes the coordination of the dithiolene ligand and accelerates the reduction process.[66] However, it is very difficult to observe the weak interactions around the active site in solution. The model study with hydrophobic substituents allows observation of noncovalent interactions in solution and investigation of the effect of the hydrophobicity of the surrounding environment by altering the polarity of the solvents.

The effect of the triarylmethyl groups

The CAr_3 groups make the complexes stable and restrict undesirable intermolecular reactions by maintaining interionic and intramolecular weak interactions. With respect to the stability of the complexes, the dioxomolybdenum(VI) complex, **2-Mo**, is much more stable than **4-Mo** with CH_3 groups. The stabilization is attributed to the bulkiness of the ligand and the intra-ligand NH···π hydrogen bond, which stabilizes the Mo–S bond. In cyclic voltammetry of **2-W**, the improved reversibility indicates the stabilization of the one electron reduced $W^{V}O_2$ species. The bulky dithiolate ligand can restrict the intermolecular side reactions.

Concerning weak interactions described in the previous section, the Et_4N^+ counterion was found close to the terminal oxo ligand of **1-M** in both the solid and solution states, and efficient uptake of Me_3NO is observed. There is a confined space around the active center that interacts with counterions or neutral small molecules. In addition, the ^{1}H NMR spectrum of **2-W** indicates that the unsymmetrical geometry remains in the hydrophobic environment even at room temperature.

In DMSOR, the huge protein is thought to stabilize the coordination of the dithiolene ligand and restrict undesirable intermolecular reactions, while the large depression enables efficient transport of the substrate to the active site. In order to understand the weak interactions and realize the catalytic activity in model systems, the inclusive design of an enzyme model is required. When the outer hydrophilic sphere of the enzyme is removed, the simplest model should contain limited space for electrostatic interactions surrounded by the hydrophobic sphere with a narrow gateway for substrate uptake. The present complexes satisfy these requirements and allow investigation of weak interactions in the hydrophobic environment.

Conclusions

Monooxomolybdenum(IV), monooxotungsten(IV), dioxomolybdenum(VI), and dioxotungsten(VI) complexes (**1-M**, **2-M**; M = Mo, W) with bulky hydrophobic dithiolate ligands and NH···S hydrogen bonds are soluble in nonpolar solvents like toluene. The thermodynamic stability of **2-M** with a *cis*-dioxo octahedral geometry is effectively enhanced by the bulkiness of the dithiolate ligands, intra-ligand bifurcated NH···S and NH···π hydrogen bonds, and the hydrophobicity of the media. The polar Me_3NO can effectively approach the active center in hydrophobic surroundings, resulting in faster oxygen-atom-transfer reaction. These results indicate that a steady structure in hydrophobic media allows observation of the unsymmetrical coordination structure and noncovalent interactions in solution. This concept of reconstructing the active site with the hydrophobic surroundings will provide new insights for enzyme modeling.

Acknowledgements

This work was supported by JSPS KAKENHI grant number 26410072.

Notes and references

1 R. Hille, J. Hall and P. Basu, *Chem. Rev.*, 2014, **114**, 3963–4038.
2 R. Hille, *Chem. Rev.*, 1996, **96**, 2757–2816.
3 R. Hille, T. Nishino and F. Bittner, *Coord. Chem. Rev.*, 2011, **255**, 1179–1205.
4 M. J. Pushie and G. N. George, *Coord. Chem. Rev.*, 2011, **255**, 1055–1084.
5 A. Magalon, J. G. Fedor, A. Walburger and J. H. Weiner, *Coord. Chem. Rev.*, 2011, **255**, 1159–1178.
6 M. K. Johnson, D. C. Rees and M. W. W. Adams, *Chem. Rev.*, 1996, **96**, 2817–2840.
7 H. Dobbek, *Coord. Chem. Rev.*, 2011, **255**, 1104–1116.
8 S. Grimaldi, B. Schoepp-Cothenet, P. Ceccaldi, B. Guigliarelli and A. Magalon, *Biochim. Biophys. Acta*, 2013, **1827**, 1048–1085.
9 H. Schindelin, C. Kisker, J. Hilton, K. V. Rajagopalan and D. C. Rees, *Science*, 1996, **272**, 1615–1621.
10 D. K. Smith and F. Diederich, *Chem. – Eur. J.*, 1998, **4**, 1353–1361.
11 C. B. Gorman and J. C. Smith, *Acc. Chem. Res.*, 2001, **34**, 60–71.
12 F. Vögtle, S. Gestermann, R. Hesse, H. Schwierz and B. Windisch, *Prog. Polym. Sci.*, 2000, **25**, 987–1041.
13 C. M. Cardona, S. Mendoza and A. E. Kaifer, *Chem. Soc. Rev.*, 2000, **29**, 37–42.
14 P. Basu, V. N. Nemykin and R. S. Sengar, *Inorg. Chem.*, 2003, **42**, 7489–7501.
15 R. L. McNaughton, S. Mondal, V. N. Nemykin, P. Basu and M. L. Kirk, *Inorg. Chem.*, 2005, **44**, 8216–8222.
16 N. Ueyama, T. Terakawa, M. Nakata and A. Nakamura, *J. Am. Chem. Soc.*, 1983, **105**, 7098–7102.
17 T. Okamura, S. Takamizawa, N. Ueyama and A. Nakamura, *Inorg. Chem.*, 1998, **37**, 18–28.
18 N. Ueyama, T. Okamura and A. Nakamura, *J. Chem. Soc., Chem. Commun.*, 1992, 1019–1020.
19 N. Ueyama, Y. Yamada, T. Okamura, S. Kimura and A. Nakamura, *Inorg. Chem.*, 1996, **35**, 6473–6484.
20 N. Ueyama, N. Nishikawa, Y. Yamada, T. Okamura and A. Nakamura, *J. Am. Chem. Soc.*, 1996, **118**, 12826–12827.

21 N. Ueyama, N. Nishikawa, Y. Yamada, T. Okamura, S. Oka, H. Sakurai and A. Nakamura, *Inorg. Chem.*, 1998, **37**, 2415–2421.
22 T. Okamura, N. Ueyama, A. Nakamura, E. W. Ainscough, A. M. Brodie and J. M. Waters, *J. Chem. Soc., Chem. Commun.*, 1993, 1658–1660.
23 K. Baba, T. Okamura, C. Suzuki, H. Yamamoto, T. Yamamoto, M. Ohama and N. Ueyama, *Inorg. Chem.*, 2006, **45**, 894–901.
24 K. Baba, T. Okamura, H. Yamamoto, T. Yamamoto, M. Ohama and N. Ueyama, *Inorg. Chem.*, 2006, **45**, 8365–8371.
25 T. Okamura, M. Tatsumi, Y. Omi, H. Yamamoto and K. Onitsuka, *Inorg. Chem.*, 2012, **51**, 11688–11697.
26 T. Okamura, K. Kunisue, Y. Omi and K. Onitsuka, *Dalton Trans.*, 2013, **42**, 7569–7578.
27 T. Okamura, Y. Ushijima, Y. Omi and K. Onitsuka, *Inorg. Chem.*, 2013, **52**, 381–394.
28 R. H. Holm, E. I. Solomon, A. Majumdar and A. Tenderholt, *Coord. Chem. Rev.*, 2011, **255**, 993–1015.
29 F. J. Hine, A. J. Taylor and C. D. Garner, *Coord. Chem. Rev.*, 2010, **254**, 1570–1579.
30 V. W. L. Ng, M. K. Taylor and C. G. Young, *Inorg. Chem.*, 2012, **51**, 3202–3211.
31 A. Majumdar and S. Sarkar, *Coord. Chem. Rev.*, 2011, **255**, 1039–1054.
32 H. Sugimoto, S. Tatemoto, K. Suyama, H. Miyake, R. P. Mtei, S. Itoh and M. L. Kirk, *Inorg. Chem.*, 2010, **49**, 5368–5370.
33 P. Basu and S. J. N. Burgmayer, *Coord. Chem. Rev.*, 2011, **255**, 1016–1038.
34 N. Yoshinaga, N. Ueyama, T. Okamura and A. Nakamura, *Chem. Lett.*, 1990, **19**, 1655–1656.
35 N. Ueyama, H. Oku, M. Kondo, T. Okamura, N. Yoshinaga and A. Nakamura, *Inorg. Chem.*, 1996, **35**, 643–650.
36 K. Baba, T. Okamura, H. Yamamoto, T. Yamamoto, M. Ohama and N. Ueyama, *Chem. Lett.*, 2005, **34**, 44–45.
37 A. G. Green and A. G. Perkin, *J. Chem. Soc.*, 1903, **83**, 1201–1212.
38 I. W. Boyd, I. G. Dance, K. S. Murray and A. G. Wedd, *Aust. J. Chem.*, 1978, **31**, 279–284.
39 G. R. Hanson, A. A. Brunette, A. C. McDonell, K. S. Murray and A. G. Wedd, *J. Am. Chem. Soc.*, 1981, **103**, 1953–1959.
40 B. Milligan and J. M. Swan, *J. Chem. Soc.*, 1962, 2172–2177.
41 F. H. Allen, V. J. Hoy, J. A. K. Howard, V. R. Thalladi, G. R. Desiraju, C. C. Wilson and G. J. McIntyre, *J. Am. Chem. Soc.*, 1997, **119**, 3477–3480.
42 C. B. Aakeroy and K. R. Seddon, *Chem. Soc. Rev.*, 1993, **22**, 397–407.
43 J. J. A. Cooney, M. D. Carducci, A. E. McElhaney, H. D. Selby and J. H. Enemark, *Inorg. Chem.*, 2002, **41**, 7086–7093.
44 H. Sugimoto, M. Tarumizu, K. Tanaka, H. Miyake and H. Tsukube, *Dalton Trans.*, 2005, 3558–3565.
45 R. Maiti, K. Nagarajan and S. Sarkar, *J. Mol. Struct.*, 2003, **656**, 169–176.
46 T. Okamura, K. Taniuchi, K. Lee, H. Yamamoto, N. Ueyama and A. Nakamura, *Inorg. Chem.*, 2006, **45**, 9374–9380.
47 S. Boyde, S. R. Ellis, C. D. Garner and W. Clegg, *J. Chem. Soc., Chem. Commun.*, 1986, 1541–1543.
48 N. Ueyama, H. Oku and A. Nakamura, *J. Am. Chem. Soc.*, 1992, **114**, 7310–7311.
49 H. Oku, N. Ueyama and A. Nakamura, *Bull. Chem. Soc. Jpn.*, 1996, **69**, 3139–3150.
50 N. Ueyama, T. Okamura and A. Nakamura, *J. Am. Chem. Soc.*, 1992, **114**, 8129–8137.
51 H. Sugimoto, M. Tarumizu, H. Miyake and H. Tsukube, *Eur. J. Inorg. Chem.*, 2007, 4663–4668.
52 A. Rodger and B. F. G. Johnson, *Inorg. Chem.*, 1988, **27**, 3061–3062.
53 A. L. Tenderholt, R. K. Szilagyi, R. H. Holm, K. O. Hodgson, B. Hedman and E. I. Solomon, *Inorg. Chem.*, 2008, **47**, 6382–6392.
54 Y. Yan, P. Chandrasekaran, J. T. Mague, S. DeBeer, S. Sproules and J. P. Donahue, *Inorg. Chem.*, 2012, **51**, 346–361.
55 J. A. Riddick, W. B. Bunger and T. K. Sakano, *Organic Solvents: Physical Properties and Methods of Purification*, Wiley, New York, 1986.
56 C. L. Hill, J. Renaud, R. H. Holm and L. E. Mortenson, *Inorg. Chem.*, 1977, **99**, 2549–2557.
57 W.-Y. Sun, N. Ueyama and A. Nakamura, *Tetrahedron*, 1992, **48**, 1557–1566.
58 R. J. Kassner and W. Yang, *J. Am. Chem. Soc.*, 1977, **99**, 4351–4355.
59 L. J. De Hayes, H. C. Faulkner, W. H. Doub and D. T. Sawyer, *Inorg. Chem.*, 1975, **14**, 2110–2116.
60 S. K. Das, D. Biswas, R. Maiti and S. Sarkar, *J. Am. Chem. Soc.*, 1996, **118**, 1387–1397.
61 A. Warshel, *Biochemistry*, 1981, **20**, 3167–3177.
62 R. Breslow, *J. Phys. Org. Chem.*, 2006, **19**, 813–822.
63 J. P. Ridge, K.-F. Aguey-Zinsou, P. V. Bernhardt, I. M. Brereton, G. R. Hanson and A. G. McEwan, *Biochemistry*, 2002, **41**, 15762–15769.
64 J. P. Ridge, K.-F. Aguey-Zinsou, P. V. Bernhardt, G. R. Hanson and A. G. McEwan, *FEBS Lett.*, 2004, **563**, 197–202.
65 A. S. McAlpine, A. G. McEwan and S. Bailey, *J. Mol. Biol.*, 1998, **275**, 613–623.
66 N. Cobb, C. Hemann, G. A. Polsinelli, J. P. Ridge, A. G. McEwan and R. Hille, *J. Biol. Chem.*, 2007, **282**, 35519–35529.

